ELSEVIER

Chemical Engineering Journal 70 (1998) 93–104

Chemical Engineering Journal

Reynolds number effects on laminar mixing in the Kenics static mixer

D.M. Hobbs, F.J. Muzzio *

Department of Chemical and Biochemical Engineering, Rutgers University, Piscataway, NJ 08855, USA

Received 19 December 1996; received in revised form 7 November 1997; accepted 7 December 1997

Abstract

The Kenics static mixer was investigated numerically using Lagrangian methods to characterize mixer performance in laminar flow. Techniques from dynamical systems analysis (Poincaré sections, tracking of fluid tracers, and the development of stretching histories for tracer elements) as well as a more traditional mixing measure (the variation coefficient) were used to compare mixing performance at various Reynolds numbers. For creeping flow conditions ($Re \leq 10$), the Kenics flow is globally chaotic and mixing performance is independent of Re. For $Re = 100$, significant islands of regular motion develop. These islands do not exchange material with the remainder of the flow and act as a barrier to uniform mixing. For $Re = 1000$, the flow is predominantly chaotic again, but small islands remain, leading to less effective mixing than under creeping flow conditions.

Keywords: Kenics static mixer; Reynolds numbers; Poincaré sections; Laminar flow; Mixing performance

1. Introduction

Mixing is an essential component of nearly all industrial chemical processes, ranging from simple blending to complex multi-phase reaction systems for which reaction rate, yield and selectivity are highly dependent upon mixing performance. Consequences of improper mixing include non-reproducible processing conditions and lowered product quality, resulting in the need for more elaborate downstream purification processes and increased waste disposal costs. Despite its importance, however, mixing performance is seldom characterized rigorously for industrial systems. Detailed characterizations are important, particularly in slow-moving laminar flows of high viscosity materials which have a serious potential to lead to inhomogeneity and poorly mixed regions within the flow system.

In recent years, significant progress has been made in the characterization of fluid–mechanical mixing using Lagrangian tracking techniques and tools from dynamical systems theory, particularly those related to chaos. The majority of previous work has focused on model flows that are two dimensional and time periodic, and a smaller set of studies have considered simple, three-dimensional, spatially periodic flows [1,2] where a simplified, two-dimensional analytical approximation to the velocity field was obtained. While complex, three-dimensional geometries typical of most industrial mixers make analytic solutions of the velocity field in such equipment impractical; a high quality numerical solution of the velocity field can provide a suitable starting point to characterize mixing performance. This approach has allowed Lagrangian techniques to be applied to a fully three-dimensional flow in a commercially relevant mixing system: the Kenics static mixer (Chemineer, Dayton, OH). Each element of the Kenics mixer is a plate which has been given a 180° helical twist. The complete mixer consists of a series of elements of alternating clockwise and counter-clockwise twist arranged axially within a pipe so that the leading edge of an element is at right angles to the trailing edge of the previous element (Fig. 1). Laminar flow in the Kenics mixer is fully three-dimensional and spatially-periodic in the axial direction, with each pair of adjacent elements forming a single periodic unit. For steady-state operation, the periodic spatial dimension in this flow is analogous to the periodic time dimension in previously studied two-dimensional flows.

Previous communications [3–5] have illustrated the use of computational fluid dynamics (CFD) to obtain the velocity field in the Kenics mixer. Mixing at low Reynolds number ($Re = 0.15$) was characterized using Lagrangian tracer tracking techniques and methods for characterizing chaotic flows [3,5]. In the remaining sections of this paper, these techniques are applied to quantitatively evaluate the mixing performance of the Kenics mixer in laminar flow for a range of Reynolds numbers up to $Re = 1000$. Section 2 briefly

* Corresponding author. Tel.: +1-908-445-3357; fax: +1-908-445-5313; e-mail: muzzio@sol.rutgers.edu

1385-8947/98/$19.00
PII S1385-8947(98)00065-5

Fig. 1. A six element Kenics static mixer.

Table 1
Mixer geometry and fluid properties

Mixer	
Diameter (D)	5.08 cm
Plate thickness	0.3175 cm
Entrance length	10.16 cm
Exit length	10.16 cm
Fluid	
Density (ρ)	1.20 g/cm^3
Viscosity (μ)	500 cp

describes the numerical techniques used to obtain the velocity fields and to characterize mixing at various Reynolds numbers. Section 3 presents results and discussion, and Section 4 summarizes the conclusions of this work.

2. Methods

2.1. Velocity field

The base configuration chosen for study was a Kenics mixer with open tube entrance and exit sections (Fig. 1). Details of the system geometry and fluid properties are given in Table 1. Simulations were performed for open tube Reynolds numbers ($\mathrm{Re}=(\rho\langle v_x\rangle D)/\mu$) of 0.15, 1, 10, 100, and 1000. The corresponding inlet velocities were $\langle v_x\rangle = 0.0012$ m/s, 0.0082 m/s, 0.082 m/s, 0.820 m/s, and 8.20 m/s, respectively. A commercially available computational fluid dynamics (CFD) software package (FLUENT/UNS©) was used to obtain the velocity field in the static mixer. Previous communications presented a full discussion of the grid generation, grid validation, and solution procedure using this software [4], and demonstrated the accuracy of the solution through comparison with experiments [3,5].

Most prior investigations of the Kenics mixer by other researchers [6–9] have neglected developing flows in order to obtain approximate analytic solutions for the velocity field. However, Eulerian characterization of the flow field and Lagrangian analysis of mixing behavior demonstrate that the flow areas neglected in such idealized analytic solutions provide the greatest potential contribution to mixer performance [4,10]. More recently, studies of the Kenics mixer [11] and the Sulzer SMRX mixer [12] by other researchers, as well as our own analyses of the Kenics mixer [3–5,10,13], have made use of CFD to obtain high quality numerical solutions for the entire velocity field, including the developing flows, without the need for additional simplifying assumptions (although such refinements come at the price of a significantly increased computational burden). In the current study, separate velocity field solutions were obtained for each Reynolds number considered (0.15, 1, 10, 100, 1000). These solutions serve as a starting point for further characterization of the mixer performance using Lagrangian tracking techniques. Such an approach has been described in detail elsewhere [3,5] and only a brief summary is presented here.

2.2. Tracking computations

Simulation software was developed to track fluid tracers as they move through the mixer flow field, using the CFD generated velocity field as input. Trajectories are tracked by integrating the vector equation of motion

$$\frac{\mathrm{d}\boldsymbol{x}}{\mathrm{d}t}=\boldsymbol{v}(\boldsymbol{x}) \tag{1}$$

for each tracer using a fourth order Runge–Kutta integration scheme with adaptive step-size control [14]. In addition to tracking the position of tracers placed into the simulated velocity field, the software is also used to compute the stretching of an infinitesimal vector $\boldsymbol{l}$ associated with each tracer. The evolution of the vector $\boldsymbol{l}$ is tracked by integrating Eq. (1) (element position) along with:

$$\frac{\mathrm{d}(\boldsymbol{l})}{\mathrm{d}t}=(\nabla\boldsymbol{v})^T\cdot\boldsymbol{l}, \qquad \boldsymbol{l}_{t=0}=\boldsymbol{l}_0 \tag{2}$$

The total accumulated stretching λ experienced by the element after some time is defined as:

$$\lambda=\frac{|\boldsymbol{l}|}{|\boldsymbol{l}_0|} \tag{3}$$

For the stretching calculations, each tracer is assigned an initial stretch vector $\boldsymbol{l}_0=[1,0,0]$. The tracer position and accumulated stretching are tracked through the flow via integration of Eqs. (1) and (2), and at each periodic plane, the position and components of the stretch vector $\boldsymbol{l}$ are recorded. The rate of intermaterial surface area generated in a region of the flow is proportional to the rate of stretching experienced by fluid tracers in that region. The stretching of fluid elements determines the rate of the micromixing process both by increasing the intermaterial area over which inter-diffusion of components can occur, and also by decreasing the required diffusional distance.

For the Reynolds numbers considered here, the Kenics velocity field shows a periodicity matching that of the mixer geometry [4]. The particle tracking software takes advantage of this periodicity to extend the simulation results from a six-element base-case mixer to devices of greater length. The six-element base case is divided into an entrance section (inlet tube and first two Kenics elements), exit section (outlet tube

and Kenics elements 5 and 6), and central periodic section (Kenics elements 3 and 4). Within the particle tracking software, the central section is repeated as a spatially periodic unit to extend the tracking to a mixer of any length.

For each Reynolds number, three types of simulations were performed. First, Poincaré sections were generated for each flow condition by tracking 15 tracers through the flow for 500 elements (250 periods) and recording their cross-sectional positions when the tracers crossed the planes after the 2nd Kenics element, 4th element, 6th element, etc. (i.e., after every spatial period). These cross-sections were then superimposed to form two-dimensional Poincaré sections. The structure of the Poincaré section reveals the nature of different flow regions. Chaotic flow regions appear as random clouds of points on the Poincaré section, while regular regions appear as areas devoid of points or closed curves. While no mixer ever has 500 elements, this computation reveals which regions of the flow domain are chaotic and which are regular, and thus determines the asymptotic degree of mixedness possible in the system. After a sufficient number of periods, trajectories that start out in the chaotic portion of the flow will asymptotically approach all points in the chaotic region, whereas trajectories that start in regular regions are confined to remain in the regular portion of the flow. Since the exchange of material between regular and chaotic portions of a flow can only occur via slow diffusion processes, the presence of regular regions presents a barrier to uniform mixing in a flow system.

The second set of tracking computations were performed to simulate mixing of equal portions of two similar fluids. In this case, ~20,000 uniformly spaced tracers were initially placed to cover the entire mixer cross-section in the open tube region 0.1 cm before the leading edge of the first Kenics element, with the points in the upper and lower halves of the cross-section assigned different colors. The tracers were tracked through the flow and their cross-sectional positions recorded when the particles crossed the planes after the 2nd Kenics element, 4th element, 6th element, etc. For these simulations, the stretching was also tracked for each tracer by integrating Eq. (2) along the tracer trajectories.

The third set of tracking computations simulated the injection of a small quantity of tracer into the bulk flow. The spreading of the tracer was quantified using the variation coefficient. Following the 'intensity of segregation' concept proposed by Danckwerts [15], mixture quality has often been quantified in terms of a mixing index that describes the degree of homogeneity of the system. The mixture homogeneity is evaluated based on a statistical analysis of samples from the mixture, with the mixing index expressed as a function of the standard deviation (σ) or variance (σ^2) of the mixture samples. A previous communication presented simulation results for mixture quality in the Kenics mixer at Re = 0.15 in terms of the variation coefficient. These results were compared with experimental results from the literature, and good agreement was obtained [3]. Due to the discrete nature of the tracer tracking results, the number-based variation coefficient $\sigma/\overline{N}$ was computed in the current study for each Reynolds number case using a procedure detailed in previous communications [10,13]. For each tracer injection simulation, approximately 10,000 uniformly spaced particles were placed in a circle centered at $(y,z) = (0,0)$, 0.1 cm upstream of the leading edge of the first Kenics element. The diameter of the circle of tracers was set such that the circle covered an area that represents 1% of the volumetric flow on the injection cross-section. The tracers were tracked through the flow, their positions recorded at every spatial period, and $\sigma/\overline{N}$ computed from the position data.

Previous communications have used the algorithms described above to analyze the flow and mixing in the Kenics mixer at Re = 0.15. Good agreement was achieved between computational results and experimental data for pressure drop [4], striation development, residence time distributions, variation coefficient [3], and a tracer mixing experiment [5]. The close correspondence between computations and experiments served to validate the simulation results and indicated that the simulations provided a good model of the physical system. The results obtained using these algorithms to investigate the flow in the Kenics mixer at other Reynolds numbers are presented and discussed next in Section 3.

3. Results

3.1. Velocity fields

The velocity fields for each Reynolds number were obtained via CFD calculations [4]. The velocity fields are illustrated in Fig. 2, which shows planar cross-sections from the third mixer element located at normalized distances of $X' = 0$, $X' = L/4$, and $X' = L/2$ relative to the length (L) of a single element. Fig. 2a–c correspond to Re = 1, d–f to Re = 10, g–i to Re = 100, and j–l to Re = 1000. The magnitude of the axial velocity is denoted by the shading of the filled contours, as indicated in the scale at the right of each set of figures (darker shades denote faster flow). The direction and relative magnitude of the radial and tangential components of the velocity are indicated by the vector field. Below Re 10, creeping flow is obtained. Under these conditions, the velocity magnitude at each flow location is directly proportional to the Reynolds number, so all creeping flow velocity fields have the same 3-dimensional structure, which is evident from Fig. 2a–c and d–f. The velocity field for Re = 0.15 [4] appears identical to that for Re = 1. For a Kenics element, the cross-sectional plane at the middle ($X' = L/2$) of the element is a plane of specular anti-symmetry. When the flow is in the creeping (reversible) regime, the velocity profiles for the cross-sectional planes at $X' = 0$ and $L/4$ are exactly analogous and anti-symmetric to the velocity profiles at $X' =$ L and 3/4 L, respectively. Developing flows are confined to ~25% of the flow at the entrance and exit of the element, and a well-developed velocity profile that is essentially constant with

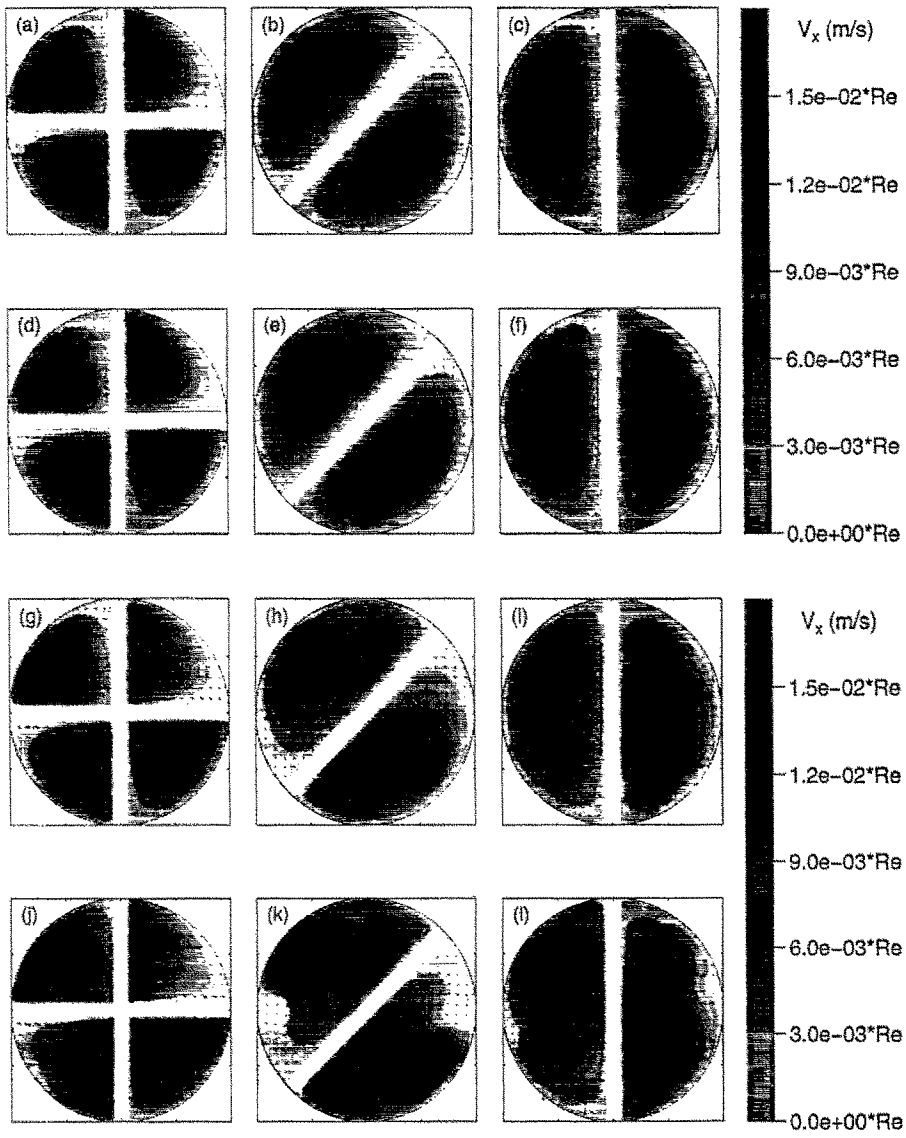

Fig. 2. Velocity fields. The filled contours represent the magnitude of axial velocity as denoted by the scale shown at the right (darker shades denote faster flow). The vector field represents the direction relative magnitude of the radial and tangential velocity components. (a)–(c) Re = 1; (d)–(f) Re = 10; (g)–(i) Re = 100; (j)–(l) Re = 1000. (a,d,g,j) $X' = 0$; (b,e,h,k) $X' = L/4$; (c,f,i,l) $X' = L/2$.

respect to the helical reference frame of the mixer element is attained in the central 75% of the element ($1/8\ L < L' < 7/8\ L$).

Above Re ≈ 10, the symmetry of the velocity field with respect to the element mid-plane is lost when inertial forces become significant and the flow is no longer reversible. At Re = 100 (Fig. 2g–i), entrance effects are significant over a larger region of the flow, extending up to $X' \approx L/2$. The transitional, developing flows persist over ~75% of the velocity profile, and only a small region of the flow attains a well-developed profile. Inertial effects become even more pronounced for Re = 1000 (Fig. 2j–l), and there is no region within a mixer element where a well-developed velocity profile is attained.

A comparison of velocity fields reveals clear differences in the Kenics flow as a function of Reynolds number. However, the effects of these velocity differences on mixing performance cannot be readily discerned from an Eulerian analysis of the velocity fields alone. An analysis of mixing performance requires Lagrangian simulations capable of capturing the evolution along the flow of partially mixed structures. The results from such computations are presented in the following sections.

3.2. Poincaré sections

The first Lagrangian tool applied to evaluate mixing performance is the Poincaré section. Poincaré sections generated at each Reynolds number using the techniques described in Section 2 are shown in Fig. 3. For Re = 0.15 (Fig. 3a), the Poincaré section appears as a nearly featureless cloud of points, suggesting that the flow is globally chaotic [5,10].

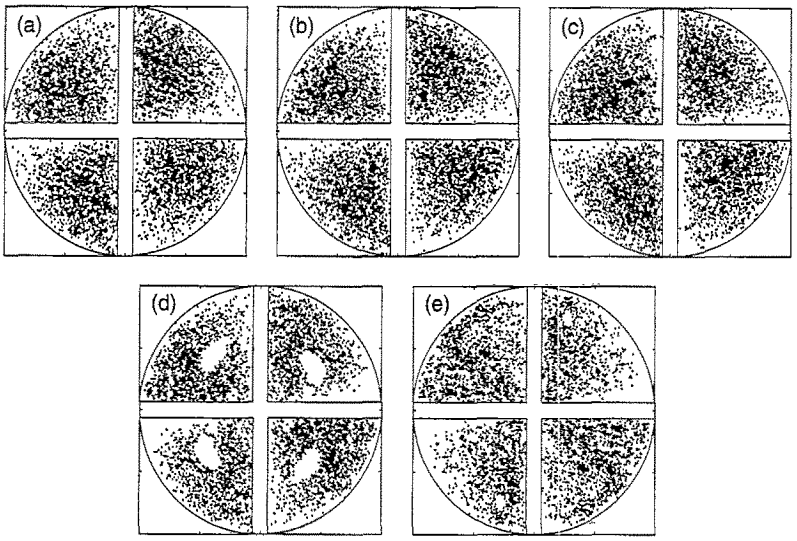

Fig. 3. Poincaré sections for (a) Re = 0.15, (b) Re = 1, (c) Re = 10, (d) Re = 100, and (e) Re = 1000.

For Re = 1 and Re = 10 (Fig. 3b and c), the Poincaré sections are similar to the Re = 0.15 case indicating that for all of the creeping flow cases, the flow remains globally chaotic.

As the Reynolds number is further increased, the structure of the Poincaré section changes. At Re = 100 (Fig. 3d), the Poincaré section has two pairs of oval-shaped regions that are devoid of points, indicating that these regions are segregated from the remainder of the flow. One pair of segregated regions is centered near $(y,z) = \pm(0.42\ R, 0.38\ R)$ in quadrants 1 and 3, and a second pair is centered near $(y,z) = \pm(-0.41\ R, 0.43\ R)$ in quadrants 2 and 4. The area outside the oval regions appears as a random sea of points, indicating chaotic flow. The area occupied by the segregated regions represents approximately 9.6% of the volumetric flow passing through the mixer. For Re = 1000 (Fig. 3e), the Poincaré section again appears as a random cloud of points with no discernible islands, suggesting that the flow is again globally chaotic.

Poincaré sections provide valuable information about the asymptotic mixing performance of the Kenics system for very long mixers. However, most applications employ mixers with a small number of elements. The tracer mixing simulations described next provide information about the evolution of partially mixed structures for situations typical of industrial applications.

3.3. Mixing simulations

Mixing of equal portions of two Newtonian fluids with identical densities and viscosities was simulated for each Reynolds number, and the structures obtained on different mixer cross-sections are shown in Fig. 4 (sub-figures a–c correspond to Re = 1, d–f to Re = 10, e–g to Re = 100, and h–j to Re = 1000). These cross-sections represent the structures which would be present at the corresponding planes for mixers in steady-state operation with a continuous feed of two segregated components. The simulation results for Re = 0.15 [3] (not shown in the interest of brevity) are identical to those for Re = 1 and also to results that have been reported in well known experimental studies [16,17]. The number of striations present in the partially mixed structure approximately doubles with each mixer element, following the standard correlation $S = 2^n$ proposed by several authors [17–19]. The simulation results for Re = 0.15 also provide good quantitative agreement with literature data for residence time distributions and variation coefficient, indicating that the simulations appear to be capturing the essential physical features of the system [3].

The striation patterns for Re = 10 (Fig. 4d–f) are essentially identical to the Re = 1 case since creeping flow behavior is retained at this Reynolds number. As mixing proceeds, the flow is divided and stretched, forming an intermeshed series of striations of the two fluids. After 10 elements (Fig. 4c and f), individual striations are no longer visible with the resolution provided by this number of tracer elements. For Re = 100 (Fig. 4g–i), distinctly different patterns are observed. At first glance, the partially mixed structure after six elements at Re = 100 (Fig. 4h) may appear somewhat more 'random' than for the lower Reynolds number flows, since the regular pattern of striations has been disrupted. However, the segregated regions identified in the Poincaré section for Re = 100 become visible as isolated regions that do not exchange material with the remainder of the flow. After 10 elements (Fig. 4i) the chaotic region appears well mixed while the segregated areas still contain only one component, revealing a significant obstacle to uniform mixing at Re = 100 that was not present at lower Reynolds numbers. As the Reynolds number is increased further to Re = 1000 (Fig. 4j–l), it is difficult to determine whether segregated regions persist in the flow. After 10 elements (Fig. 4l), the flow appears well mixed and no segregated islands can be detected visually with the degree of resolution provided by the number of tracers used.

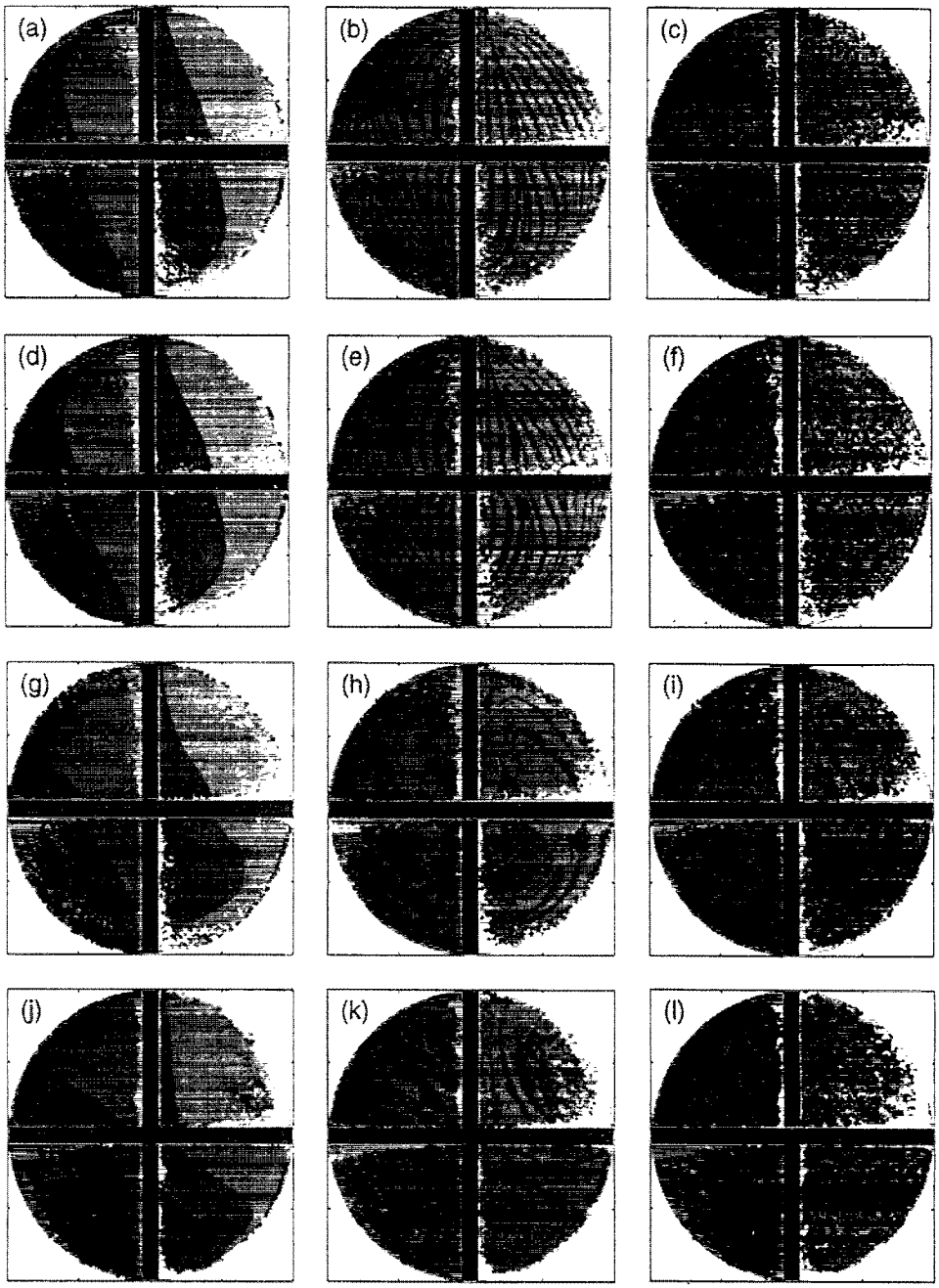

Fig. 4. Equal volume mixing of two initially segregated components. (a)–(c) Re = 1; (d)–(f) Re = 10; (g)–(i) Re = 100; (j)–(l) Re = 1000. Cross-sectional slices for two elements (a,d,g,j); six elements (b,e,h,k); and 10 elements (c,f,i,l).

3.4. Variation coefficient

While the evolution of striation patterns provides a valuable qualitative understanding of mixing progress within the static mixer, a quantitative description of the mixture quality provides a more practical means of evaluating mixer performance. In order to quantify differences in mixing performance at different Reynolds numbers, a 1% tracer injection was simulated in each flow for tracer material with the same density and viscosity as the bulk fluid. The tracer injection was centered at $(y,z) = (0,0)$, 0.1 cm upstream of the edge of the first element. Representative cross-sections from the tracer tracking are shown in Fig. 5. Fig. 5a–c show cross-sections for Re = 10; the results for Re < 10 (not shown) appear identical to the Re = 10 case. With progress through the mixer, the initial circle of points is stretched into a ribbon, which is elongated, re-oriented, and folded by the flow within individual elements, and cut by the leading edges of sequential mixer elements. The tracer is initially confined to a small fraction of the total flow, but is redistributed by the mixing action to spread throughout the flow domain after 12 elements (Fig. 5c). The results of similar tracer studies for the Re = 100 and Re = 1000 cases are shown in Fig. 5d–f and g–i, respectively. In the Re = 100 case, the tracer spreads to most of the chaotic

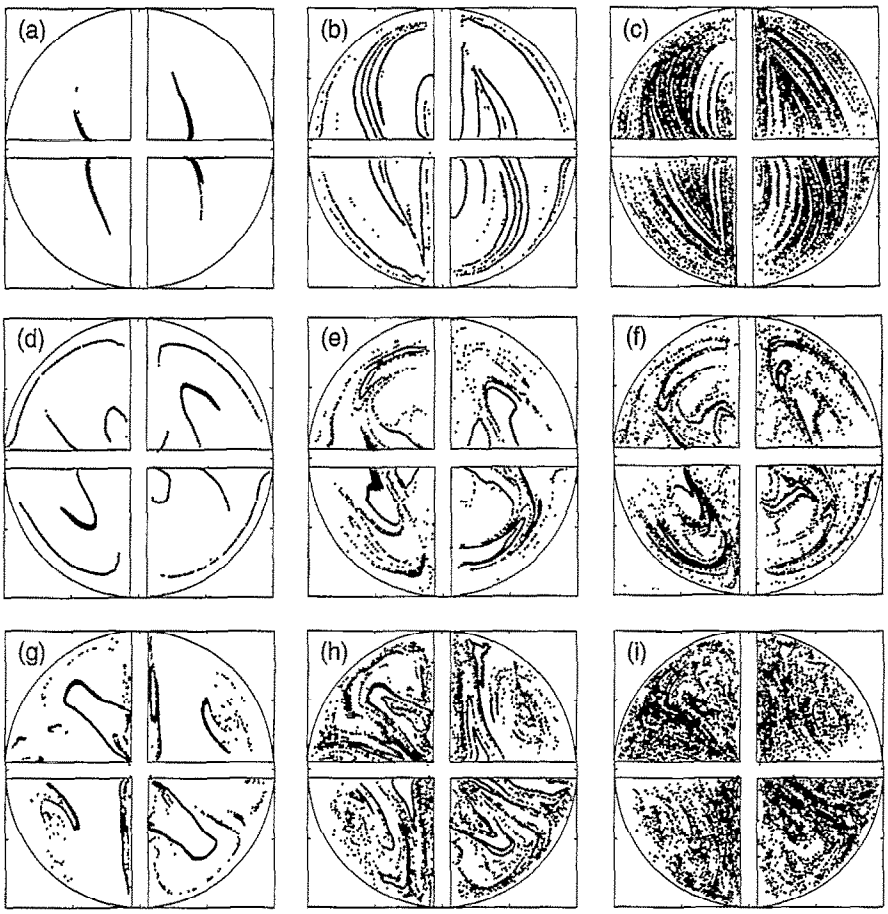

Fig. 5. Cross-sectional profiles for 1% tracer injection at $y=0$, $z=0$. (a–c) Re = 10, (d–f) Re = 100, (g–i) Re = 1000. Cross-sectional slices for four elements (a,d,g); eight elements (b,e,h); and 12 elements (c,f,i).

region after approximately 12 elements (Fig. 5f). However, the small segregated regions identified in Fig. 4i remain devoid of tracer. For Re = 1000, the tracer again spreads throughout the flow after 12 elements. While the flow for Re = 10 appears to provide the best mixing, such a qualitative, 'eye-ball' statement needs to be challenged by quantitative means.

From the tracer mixing simulations, the number-based variation coefficient was computed for each Reynolds number. The results $\sigma/\overline{N}$ vs. normalized axial position X are shown in Fig. 6. For all Re, the calculated variation coefficient decreases monotonically from the inlet up to $X=15$ tube diameters (10 mixer elements). After this point, the variation coefficient levels out, indicating that the characteristic length for the mixture has fallen below the scale of the grid size used for calculation, and further homogenization of the mixture cannot be determined at this level of resolution. Increasing the resolution of the variation coefficient by two mixer elements would require a sixteen-fold increase in the number of tracked particles, and a corresponding increase in the computation time (to approximately 1000 h of CPU time on a Sun SPARC 20/712) [3]. However, the variation coefficient data for the first 10 mixer elements is sufficient for further comparisons and the marginal increase in the resolution that could be obtained with more extensive computations does not justify the increase in computational time.

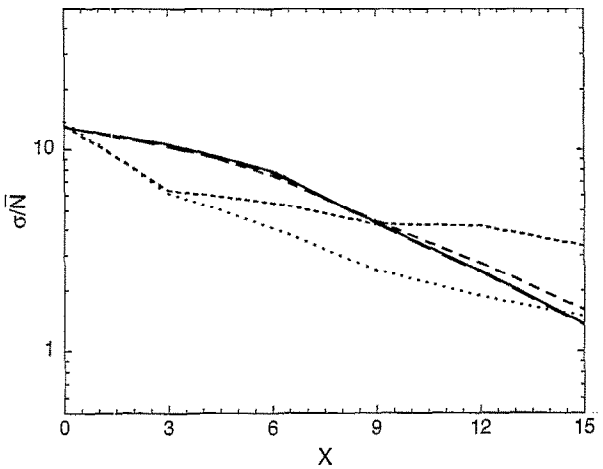

Fig. 6. Variation coefficient vs. normalized axial position X. (——— Re = 0.15; —·—·— Re = 1; — — — Re = 10; - - - - - Re = 100; ····· Re = 1000).

For Re ≤ 10, the variation coefficient curves are essentially identical, indicating equivalent mixing performance per unit length. For Re = 100, the variation coefficient drops more rapidly than for the creeping flow cases over the first two

elements, but subsequently, the rate of reduction slows down. The final asymptotic variation coefficient achieved for the Re = 100 case is greater than the asymptotic value under creeping flow conditions, due to the presence of the unmixed islands which prevent an even distribution of tracer in the Re = 100 case. For Re = 1000, the variation coefficient drops more rapidly than the creeping flow cases for the first two elements, after which it decreases more slowly than for the creeping flow case. After 10 elements, the final variation coefficient values achieved for Re = 1000 and Re ≤ 10 are approximately the same.

The variation coefficient results presented in Fig. 6 are for a single tracer injection location along the centerline of the mixer. Shifting the injection point to another location in the flow would have some effect on the results, but would not affect the conclusions about the relative mixing performance of each case. Under creeping flow conditions, injection location has an effect on the extent of mixing only for the first few elements, after which the rate of mixing is independent of injection location [13] (all flows with Re ≤ 10 would still produce identical results at any chosen injection point). For the Re = 1000 flow as well, the choice of injection location would only affect the variation coefficient results over the first few elements. Due to the chaotic nature of the flow, material injected at any location eventually spreads to the entire flow. For Re = 100, tracer injected at any point in the chaotic portion of the flow spreads throughout the chaotic region, producing the same asymptotic variation coefficient as in Fig. 6. However, if tracer were injected inside one of the regular islands, the tracer would remain trapped in the island would not spread to the chaotic portion of the flow, resulting in a more highly segregated system and a greater asymptotic value for the variation coefficient.

A quantitative comparison of the different Reynolds number cases was made by fitting the variation coefficient results for the first 10 mixer elements to an equation of the form:

$$\frac{\sigma}{N} = A \exp(-BX) \tag{4}$$

which is frequently used to describe data of this type [20]. The coefficient B represents the rate of decrease in the variation coefficient per unit mixer length and provides a quantitative measure of the rate of mixing. For the three creeping flow cases, equivalent mixing rates are achieved and $B = 0.17$ for each case. For Re = 100 and Re = 1000, $B = 0.05$ and $B = 0.12$, respectively, indicating that these cases produce slower mixing per axial distance than the creeping flow conditions.

The energy required to mix a volume of fluid in a static mixer is directly proportional to the system pressure drop, which in turn is a function of the flow Reynolds number. For Re ≤ 10, the pressure drop in the Kenics mixer is directly proportional to the Reynolds number [4]; for 10 < Re < 1000, the pressure drop is approximately proportional to $Re^{3/2}$. Since equivalent mixing rates are obtained for all flows with Re ≤ 10, the most energy efficient mixing is achieved at the lowest values of Re. Flows above Re = 10 produce less effective mixing at an even higher energy cost. This is in direct contrast to the common generalization that 'better' mixing is achieved at higher Reynolds numbers. A previous study of heat and mass transfer in the Kenics mixer by other investigators [21] indicated an analogous trend: as Reynolds number increased, heat transfer efficiency decreased since only a minimal rise in heat transfer coefficient was achieved at the expense of a significant increase in pressure drop. Although energy efficiency is maximized as Re → 0, this obviously does not represent a realistic operating condition since it also leads to infinite residence times and zero process throughput. In practical applications, the energy requirement must be balanced against other process considerations such as the residence time required to give a desired product distribution to determine the optimal operating conditions.

3.5. Stretching

Computations of stretching provide another means of quantifying mixing performance. For the tracer mixing simulations shown in Fig. 5, stretching was also computed along the tracer trajectories via Eq. (2). The geometric mean stretching $\langle\lambda\rangle$ was computed as a function of axial position for each Reynolds number, and the results are shown in Fig. 7. The mean stretch grows at a steady exponential rate vs. the number of mixer elements for each Reynolds number considered. This exponential growth of stretching, which corresponds to an exponential generation of intermaterial area as fluid flows through the mixer, is one of the defining features of a chaotic flow. The exponential stretching rate can be described in terms of a specific stretching rate per period, α, computed as:

$$\alpha = \lim_{n\to\infty}\left[\frac{1}{n}\ln\langle\lambda\rangle\right] \tag{5}$$

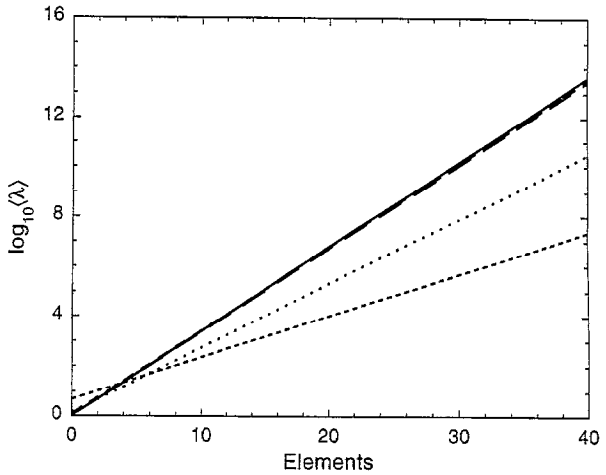

Fig. 7. Mean ($A_n = \log_{10}\langle\lambda\rangle$) of the logarithm of stretching vs. normalized axial position X. (——— Re = 0.15; —— —— Re = 1; — — — Re = 10; - - - - - Re = 100; · · · · · Re = 1000).

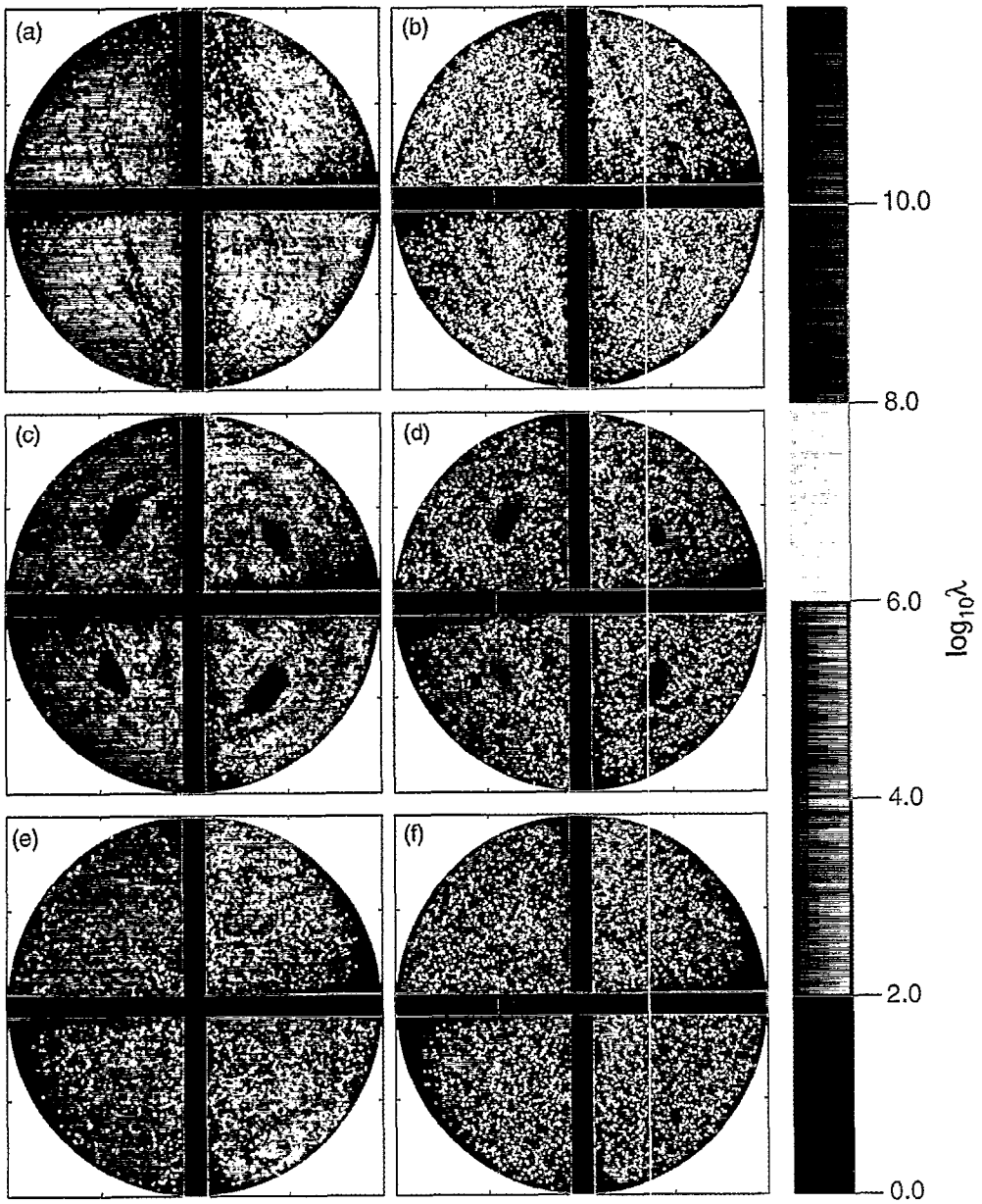

Fig. 8. Cross-sectional profiles of the logarithm of stretching, $\log_{10}\lambda$. The magnitude of $\log_{10}\lambda$ is represented by the color scale at right. (a, b) Re = 10, (c, d) Re = 100, (e, f) Re = 1000. Cross-sectional slices for 12 elements (a,c,e), and 24 elements (b,d,f).

The specific stretching rate for a spatially-periodic flow is the direct analog of the Lyapunov exponent in a time periodic system. For $Re \leq 10$, the specific stretching rates are nearly identical, and $\alpha = 1.63 \pm 0.01$ for the three cases considered. For Re = 100 and 1000, lower average stretching rates of 0.75 and 1.18, respectively, are found. The specific stretching rates for each case are consistent with the results for variation coefficient. The results from both techniques indicate that the creeping flow cases ($Re \leq 10$) produce the highest rates of mixing (which are also independent of Re), the Re = 100 case provides the slowest mixing rate, and the Re = 1000 case is intermediate between the two.

The overall structure of the stretching fields for each flow can also be examined. Plots of the spatial distribution of stretching at several mixer cross-section are shown in Fig. 8-a,b for Re = 10 (again, the results for $Re \leq 10$ are all identical). The positions of the dots correspond to the cross-sectional position where the tracked tracers cross the plane. The color of the dots represents the logarithm of the stretching magnitude, $\log_{10}(\lambda)$, where λ is calculated via Eq. (3). The color scheme is shown at the right of the figure: dark blue and light blue correspond to low stretching, green and yellow to intermediate values, and magenta and red to the highest stretching. A general increase in stretching values with progress through the mixer is evident, consistent with the exponential growth in mean stretching shown in Fig. 6. A distribution of stretching values is observed, with some regions exhibiting stretching significantly higher than the mean (red and yellow areas in Fig. 8a) while other regions exhibit stretching below the mean (green areas in Fig. 8b).

Similar cross-sections are shown in Fig. 8c,d for Re = 100. For this case, the same type of general increase in stretching is evident in the chaotic portion of the flow. In the regular islands, however, extremely low relative stretching is observed which does not exhibit the same rate of increase as the stretching in the chaotic region. For Re = 1000 (Fig. 8d,e), the stretching field appears more uniform again, and no islands of low stretching are visible.

Differences in stretching behavior for each Reynolds number may be examined statistically by computing distributions of the stretching magnitudes. Stretching distributions have been examined previously for the Kenics mixer at very low Reynolds numbers [3,5]. Due to the exponential increase of stretching in chaotic regions, the distribution of λ values are best described using the probability density function of the logarithm of stretching values $H_n(\log_{10}\lambda) = (1/N)\, dN(\log_{10}\lambda)/d\log_{10}\lambda$, which is computed for each periodic plane by counting the number of points $dN(\log_{10}\lambda)$ that have stretching values between $\log_{10}\lambda$ and $\log_{10}\lambda + d(\log_{10}\lambda)$. Conceptually, $H_n(\log_{10}\lambda)$ can be interpreted as a spectrum of intensities in the micromixing process. Fig. 9 shows plots of $H_n(\log_{10}\lambda)$; subfigures a, b, c, and d correspond to Re = 1, 10, 100, and 1000. Each plot contains several curves, corresponding to different mixer cross-sections (periodic planes after 4, 12, 20, 28, 36, and 44 mixer elements).

The $H_n(\log_{10}\lambda)$ vs. $\log_{10}\lambda$ plots obtained for Re = 1 and Re = 10 (Fig. 9a and b) are identical to one another and to the results previously obtained for the Kenics flow at Re = 0.15 [5]. As the number of mixer elements increases, stretching accumulates and the curves shift toward higher values of $\log_{10}\lambda$. After the first few elements, the central portion of the curve begins to approach a bell-shaped, Gaussian profile which describes the spectrum of stretching intensities for the bulk of the flow. Such distributions are typical of chaotic flows [22–24]. The $H_n(\log_{10}\lambda)$ curves for the creeping flow cases also exhibit long non-Gaussian tails on the high stretching side, indicating that a subset of points experiences very high stretching. The high stretching regions of the Kenics flow that produce tailing in the $H_n(\log_{10}\lambda)$ curves under creeping flow conditions were characterized for the Re = 0.15 case, and were found to coincide with the unstable manifolds of two hyperbolic period-1 points located at $(y,z) = \pm(0.13\,R, 0.98\,R)$ in the mixer cross-section on the plane between periodic segments [5]. The dominant feature of the unstable manifold of the period-1 point in quadrant 1 is a streak that emanates from the point and stretches down

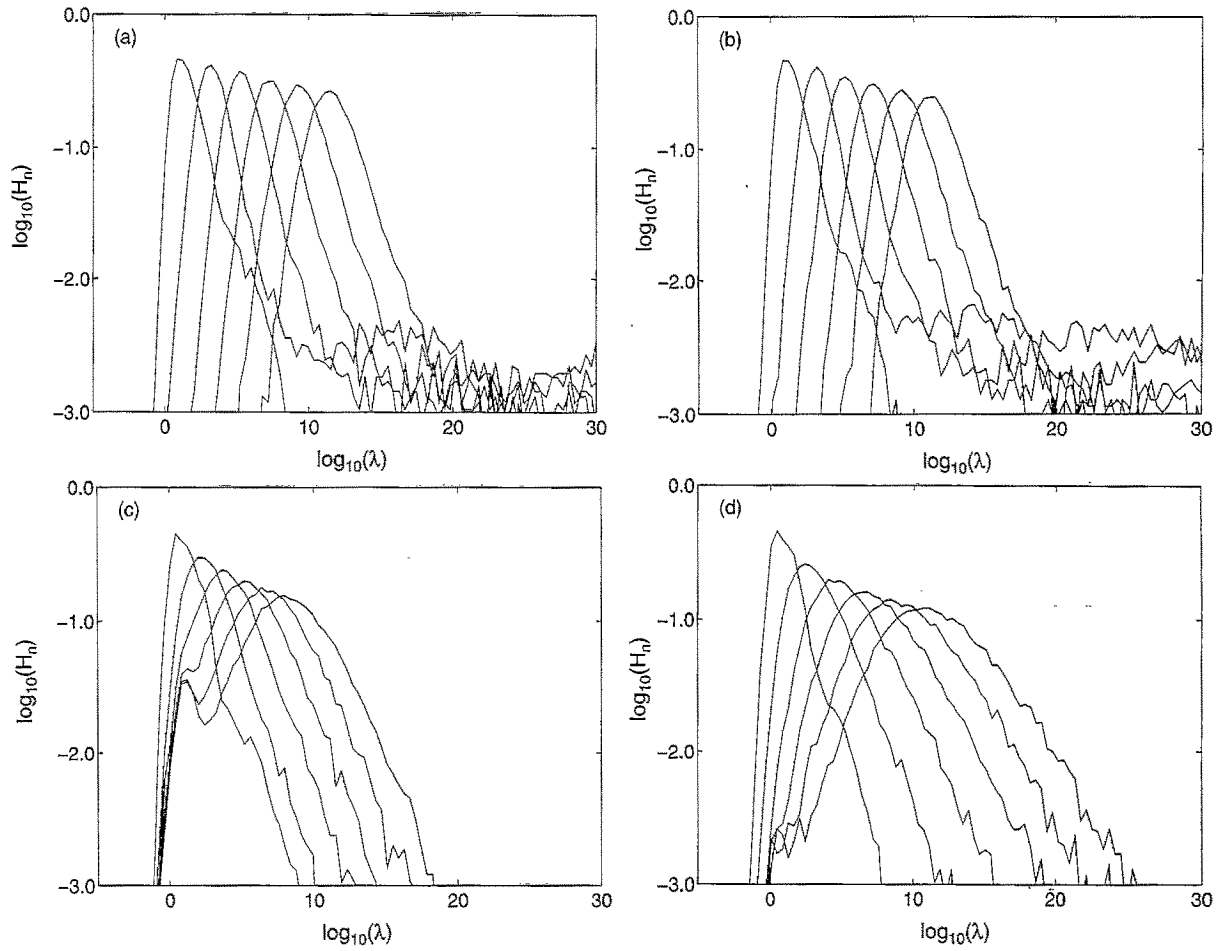

Fig. 9. Probability density function of the logarithm of stretching values, $H_n(\log_{10}\lambda)$, plotted for 4, 12, 20, 28, 36, and 44 elements. The curves shift from left to right as the number of mixer elements is increased. (a) Re = 1; (b) Re = 10; (c) Re = 100; (d) Re = 1000.

and to the right across the flow cross-section, with a symmetric streak for the quadrant 3 period-1 point. This structure corresponds exactly to the highest stretching regions in Fig. 8a,b.

For Re = 100 (Fig. 9c), the $H_n(\log_{10}\lambda)$ curves have a different shape and the distributions now display two distinct regions. A broad Gaussian profile develops on the right-hand side of the curves and shifts to the right toward higher values of $\log_{10}\lambda$ as the number of mixer elements increases. The second region of the curves is a sharper peak at the low-stretch side of the plot which does not move as rapidly toward higher stretching values as the number of elements is increased. The stretching distributions in Fig. 9c appear qualitatively similar to distributions obtained for flows that exhibit a mixture of chaotic regions and regular islands [22,25,26]. Stretching grows exponentially for points in the chaotic portion of the flow, and these stretching values correspond to the roughly Gaussian region of the $H_n(\log_{10}\lambda)$ curves. For points in the regular islands, stretching only grows linearly with progress through the mixer, and these stretching values correspond to the low stretch peak.

For Re = 1000 (Fig. 9d), the stretching distribution is again dominated by a single broad Gaussian peak. However, the small 'bumps' on the low stretching side of the distribution suggests that some very small islands may be present in the flow for Re = 1000, even though islands were not visible from Poincaré sections or tracer mixing patterns. In this case, the stretching distributions provide a more sensitive tool for detecting the presence of small low stretching regions than the cross-sectional plots, which are more limited by graphical resolution and the number of tracer elements used.

Differences among the stretching distributions for the various Reynolds numbers are highlighted in Fig. 10 by plotting the PDF for each case after 40 elements. For Re ≤ 10, the distributions are essentially identical, consisting of a single compact peak with extended tailing on the high stretching side of the distributions (minor differences in the high-stretch tails of the distributions are due to noise). For Re = 100, along with the addition of the low-stretching peak, the Gaussian portion of the distribution is broader than for the creeping flow cases and is shifted toward lower stretching values. Also, there is less tailing on the high stretching side of the distribution. For Re = 1000, the Gaussian portion of the distribution is considerably broader than for the Re ≤ 10 cases and covers a wider range of stretching intensities. The mode of the curve is shifted slightly to the left relative to creeping flow, toward lower stretching values, and the distribution lacks a pronounced high stretching tail.

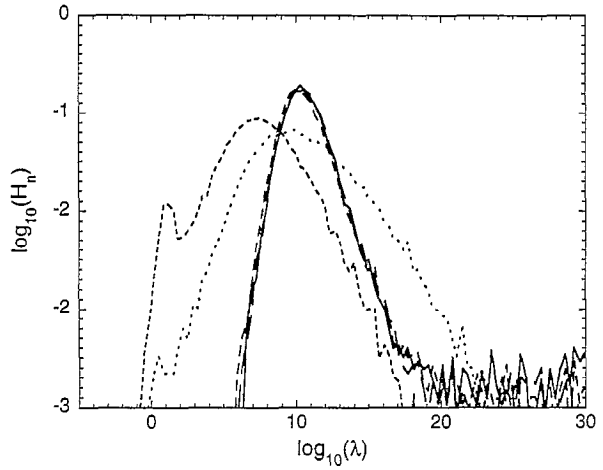

Fig. 10. Probability density function of the logarithm of stretching values, $H_n(\log_{10}\lambda)$, plotted for 40 elements. (——— Re = 0.15; —— —— Re = 1; — — — Re = 10; - - - - - Re = 100; · · · · · Re = 1000).

4. Conclusions

Kenics mixer performance was investigated as a function of Reynolds number in the laminar flow regime (Re ≤ 1000) for Newtonian fluids with constant density and viscosity. For each case, Lagrangian tracking simulations were performed to compute position and stretching for a large number of fluid tracers placed into the flow. Poincaré sections were generated to identify regions of chaos and regularity in the flow and to examine asymptotic mixing behavior. Mixing simulations for initially segregated fluids and for tracer injections provided qualitative images of mixing progress and quantitative data for computation of the variation coefficient as a function of axial position. Stretching computations provided an additional quantitative measure of micromixing intensity for different Reynolds number cases.

The simulation results from this study characterize Kenics mixer performance at several discrete Reynolds numbers and provide a general guideline for the effectiveness of the Kenics mixer under different flow conditions. Among the cases examined, stretching and variation coefficient computations both indicate that the most effective mixing is achieved for creeping flow conditions (Re ≤ 10), with poorer performance at Re = 100 and Re = 1000. The Kenics flow appears to be globally chaotic in the creeping flow regime (Re ≤ 10), but regular islands develop at Re = 100 which encompass almost 10% of the volumetric flow in the mixer. The regular islands in the flow present a significant barrier to uniform mixing and their presence suggests that the Kenics mixer is less effective in laminar flow applications above Re ≈ 10. At Re = 1000, the islands have decreased in size and are not detectable in tracer mixing simulations; however, the presence of a 'bump' of low stretching values in the distribution suggests that small islands still persist. Additional computational and experimental investigation of Kenics performance above Re = 10 is needed to determine the range of Reynolds numbers for which the regular islands have a significant impact on mixing in the system. The impact of the segregated islands on other variables, such as heat or mass transfer in the Kenics, would also be of interest.

Below Re = 10, equivalent mixing per axial distance is achieved for all flow conditions. In this flow regime, the work expended per unit volume passing through the mixer is proportional to the Reynolds number, and the most energy effi-

cient mixing is achieved at the lowest flowrates. However, energy requirements must be balanced against considerations of productivity and allowable residence times to determine the optimum operating conditions.

The results obtained from study of the Kenics mixer further demonstrate that dynamical systems analysis tools can be applied for the analysis of mixing in real, industrially-relevant systems. Tracer mixing simulations and stretch tracking are practical computational tools to quantitatively analyze mixer performance under different conditions before undertaking costly experimental investigation. The Lagrangian tracking tools that have been developed could also be applied to other properties of interest for the flow system, such as heat or mass transfer, striation thickness distributions, and chemical reactions. Work in these areas is in progress in our laboratory and will be presented in future communications.

5. Nomenclature

A	Intercept parameter for variation coefficient
B	Slope parameter representing the rate of decrease of the coefficient of variation per mixer length
D	Tube diameter
l	Fluid filament vector tracked for stretching computations
l_0	Initial condition for vector l
L	Axial length of a single mixer element
n	Period
R	Mixer radius
Re	Empty tube Reynolds number $= (\rho\langle v_x\rangle D)/\mu$
$v(x)$	Particle velocity as a function of position
∇v	Velocity gradient
X	Axial position normalized by tube diameter D
X'	Normalized axial position within a single mixer element
x	Vector of particle position (x, y, z)

Greek letters

Λ_n	Logarithm of geometric mean stretching $= \log_{10}\langle\lambda\rangle$
λ	Stretching experienced by vector l
$\langle\lambda\rangle$	Geometric mean of stretching over all vectors on a given cross-section
μ	Fluid viscosity
ρ	Fluid density
σ^2	Variance
σ	Standard deviation
$\sigma/\bar{N}$	Number based variation coefficient

Acknowledgements

This work was supported by awards from NSF (CTS 94-14460), from 3M, and from Dupont to FJM. DMH is grateful to Merck for support during the performance of this work.

References

[1] D.V. Khakhar, J.G. Franjione, J.M. Ottino, A case study of chaotic mixing in deterministic flows: the partitioned-pipe mixer, Chem. Eng. Sci. 42 (1987) 2909.
[2] H.A. Kusch, J.M. Ottino, Experiments on mixing in continuous chaotic flows, J. Fluid Mech. 236 (1992) 319.
[3] D.M. Hobbs, F.J. Muzzio, The Kenics static mixer: a three-dimensional chaotic flow, Chem. Eng. J. (1997) to appear.
[4] D.M. Hobbs, P.D. Swanson, F.J. Muzzio, Numerical characterization of low reynolds number flow in the Kenics static mixer, Chem. Eng. Sci. (1997) to appear.
[5] D.M. Hobbs, M.M. Alvarez, F.J. Muzzio, Mixing in globally chaotic flows: a self-similar process, Fractals (1997) to appear.
[6] J. Arimond, L. Erwin, Modeling of continuous mixers in polymer processing, J. Eng. Ind.-Trans. ASME 107 (1985) 70.
[7] J. Arimond, L. Erwin, A simulation of a motionless mixer, Chem. Eng. Commun. 37 (1985) 105.
[8] K. Dackson, E.B. Nauman, Fully developed flow in twisted tapes: a model for motionless mixing, Chem. Eng. Commun. 54 (1987) 381.
[9] F.H. Ling, X. Zhang, A numerical study on mixing in the Kenics static mixer, Chem. Eng. Commun. 136 (1995) 119.
[10] D.M. Hobbs, F.J. Muzzio, Optimization of a static mixer using dynamical systems techniques, submitted to Chem. Eng. Sci., 1997.
[11] T. Avalosse, M.J. Crochet, Finite-element simulation of mixing: 2. Three-dimensional flow through a Kenics mixer, AIChE J. 43 (1997) 588.
[12] E.S. Mickaily-Huber, F. Bertrand, P. Tanguy, T. Meyer, A. Renken, F.S. Rys, M. Wehrli, Numerical simulations of mixing in an SMRX static mixer, Chem. Eng. J. 63 (1996) 117.
[13] D.M. Hobbs, F.J. Muzzio, Effects of injection location, flow ratio and geometry on Kenics mixer performance, AIChE J. (1997) to appear.
[14] W.H. Press, B.P. Flannery, S.A. Teukolsky, W.T. Vetterling, Numerical Recipes, The Art of Scientific Computing, Cambridge Univ. Press, Cambridge, 1986.
[15] P.V. Danckwerts, The definition and measurement of some characteristics of mixtures, Appl. Sci. Res. A 3 (1952) 279.
[16] C.D. Grace, Static mixing and heat transfer, Chem. Proc. Eng. (1971) 57.
[17] S. Middleman, Fundamentals of Polymer Processing, McGraw-Hill, New York, 1977.
[18] S.J. Chen, In-line, continuous mixing and processing of cosmetic products, J. Soc. Cosmet. Chem. 24 (1973) 639.
[19] Z. Tadmor, C.G. Gogos, Principles of Polymer Processing, Wiley, New York, 1979.
[20] J.C. Godfrey, Static mixers, in: N. Harnby, M.F. Edwards, A.W. Nienow (Eds.), Mixing in the Process Industries, Butterworth–Heinemann, Oxford, 1992, 225.
[21] P. Joshi, K.D.P. Nigam, E.B. Nauman, The Kenics static mixer: new data and proposed correlations, Chem. Eng. J. 59 (1995) 265.
[22] F.J. Muzzio, C. Meneveau, P.D. Swanson, J.M. Ottino, Scaling and multifractal properties of mixing in chaotic flows, Phys. Fluids A 4 (1992) 1439.
[23] M. Liu, R.L. Peskin, F.J. Muzzio, C.W. Leong, Structure of the stretching field in chaotic cavity flows, AIChE J. 40 (1994) 1273.
[24] M. Liu, F.J. Muzzio, R.L. Peskin, Effects of manifolds and corner singularities on stretching in chaotic cavity flows, Chaos, Sol., Fract. 4 (1994) 2145.
[25] F.J. Muzzio, P.D. Swanson, J.M. Ottino, The statistics of stretching and stirring in chaotic flows, Phys. Fluids A 3 (1991) 822.
[26] F.J. Muzzio, P.D. Swanson, J.M. Ottino, Mixing distributions produced by multiplicative stretching in chaotic flows, Int. J. Bifurc. Chaos 2 (1992) 37.